Focussed on: Fracture and Structural Integrity related Issues

# FE analysis of cruciform welded joints considering different mechanical properties for base material, heat affected zone and weld metal

Pasqualino Corigliano, Vincenzo Crupi, Eugenio Guglielmino
*Department of Electronic Engineering, Chemistry and Industrial Engineering, University of Messina, Contrada di Dio - 98166 - Sant'Agata, Messina, Italy*
*pcorigliano@unime.it, crupi.vincenzo@unime.it, eguglie@unime.it*

Wolfgang Fricke
*Hamburg University of Technology. Institut für Konstruktion und Festigkeit von Schiffen*
*w.fricke@tu-harburg.de*

**ABSTRACT.** The aim of this scientific work was to investigate the behaviour of cruciform welded joints under static loading using a full-field technique: Digital Image Correlation. The material curves, relative to different zones (base material, heat affected zone, weld), were obtained by hardness measurements, which were done by means of a fully automated hardness scanner with high resolution. This innovative technique, based on the UCI method, allowed to identify the different zones and to assess their different mechanical properties, which were considered in the finite element model. Finally the finite element model was validated experimentally, comparing the results with the measurements obtained using the Digital Image Correlation technique.

**KEYWORDS.** Cruciform welded joints; Ship structures; Hardness measurements; Digital Image Correlation; FE analysis.

## INTRODUCTION

Welds sometimes represent a weak point, due to the presence of possible crack-like defects along with high stress concentration effects and tensile residual stresses caused by the thermal welding process itself. The strength of welded structures reduces in presence of fatigue loading. The literature on fatigue analysis of welded joints was reviewed in [1, 2]. The fatigue strength of welded joints in high cycle fatigue (HCF) [4] and low cycle fatigue (LCF) [5] regimes was already investigated by the authors. The assessment of the fatigue strength becomes more complex in presence of a multiaxial stress state [6, 7] and complex structures [8]. The welding process induces variations depending also on microstructural factors. The local mechanical properties are expected to change from the melted to the heat affected zone and generally they will be different from the base material ones [3]. Local approaches are applied in these cases and are mainly based on local displacement and strain measurements by strain gauges.
The aim of this scientific work was to investigate the behaviour of cruciform welded joints under static loading, considering the different material properties of base material (BM), heat affected zone (HAZ) and weld metal (WM). The material curves, relative to the different zones were obtained by hardness measurements, which were done by means of a

fully automated hardness scanner with high resolution, and were considered in the FE analysis. The FE model was validated by means of the results obtained using a full-field technique: Digital Image Correlation (DIC).

## MATERIALS AND METHODS

The investigated cruciform joint, shown in Fig. 1, is made of S235JR mild steel, which is commonly applied in shipbuilding. Its nominal dimensions are reported in Fig. 2, misalignment is around 1 mm. Full-penetration welding was performed using the MAG process. Tensile tests were carried out on specimens made of the same steel and quasi-static tests in displacement control on welded joints.

Figure 1: Cruciform welded joint.

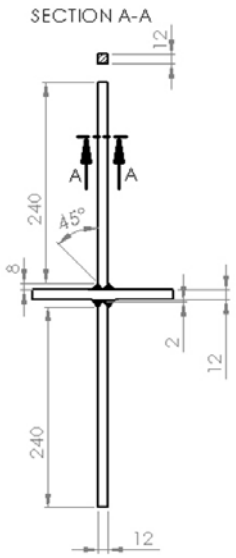


Figure 2: Specimen geometry.

## RESULTS AND DISCUSSION

### *Hardness Measurements*

The specimen was polished and it was possible to see the three different zones of the material (BM, HAZ, WZ) depicted in Fig. 3. Hardness measurements were performed at the Helmholtz-Zentrum in Geesthacht-Germany, using the Ultrasonic Contact Impedance (UCI) method. The UCI method is based on the natural resonance frequency of a bar, which pushes the Vickers diamond to penetrate into the sample. The measured frequency change depends on the size of the contact surface between the diamond and the sample for a fixed test load, which is related to the hardness of the sample. The aim of the present investigation was to investigate how hardness values influence the global behavior of the weld. The measurements (Fig. 4) showed few zones with different hardness values. Different groups of hardness measurements were identified and they are shown in Fig. 5.

The relationship between the ultimate strength $\sigma_u$ (in MPa) and HB hardness can be described by a second-order polynomial equation proposed in [9] and given by:

$$\sigma_u = 0.0012 \cdot HB^2 + 3.3 \cdot HB \quad (1)$$

This equation is a better approximation, especially for high hardness values, than the commonly used linear relations. The yield strength $\sigma_y$ was also found as a function of the Brinell hardness (HB) according to the following equation [9]:

$$\sigma_u = 0.0039 \cdot HB^2 + 1.62 \cdot HB \quad (2)$$

Four groups of hardness were used to define different σ-ε curves. In particular HV=140-160 was found to be coherent with respect to the experimental σ-ε curves previously performed on specimens, made of the same steel, and it was used for the assessment of the base material properties; values of HV=190, 230 and 270 were used for the heat affected zones and welded zones. HV values were first converted in HB hardness, then static tensile properties were calculated and reported in Tab. 1. Finally the true σ-ε curves were evaluated. The elastic strains (for $\sigma < \sigma_y$) were simply calculated as $\sigma/E$; while the elastic-plastic strains (for $\sigma > \sigma_y$) were taken from the Ramberg-Osgood equation and the parameters were calibrated using the experimental σ-ε curve of the base material, keeping the horizontal Lüder's plateau. Fig. 6 shows the material curves, obtained by hardness measurements and by tensile test carried out on a specimen made of the same steel. The hardest fillet weld could be the last one which was made during the welding process because the heat input may affect the hardness of the previously welded ones.

Figure 3: Different material zones.

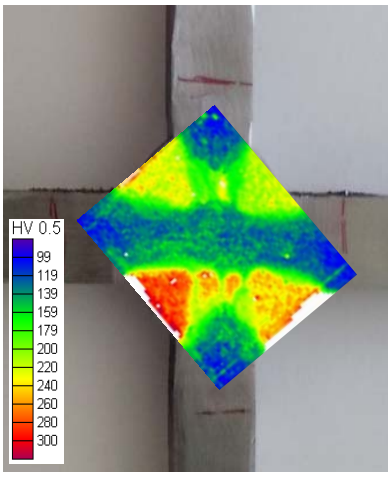


Figure 4: Hardness measurements.

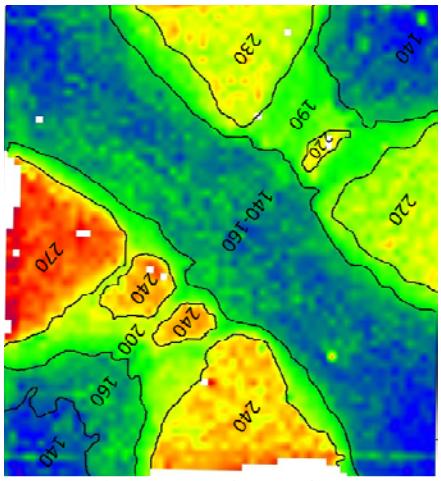


Figure 5: Hardness values.

| HV | $\sigma_y$ [MPa] | $\sigma_u$ [MPa] | E [MPa] |
|---|---|---|---|
| 140 | 300 | 460 | 205000 |
| 190 | 421 | 636 | |
| 230 | 542 | 780 | |
| 270 | 656 | 908 | |

Table 1: Hardness measurements and related mechanical properties.

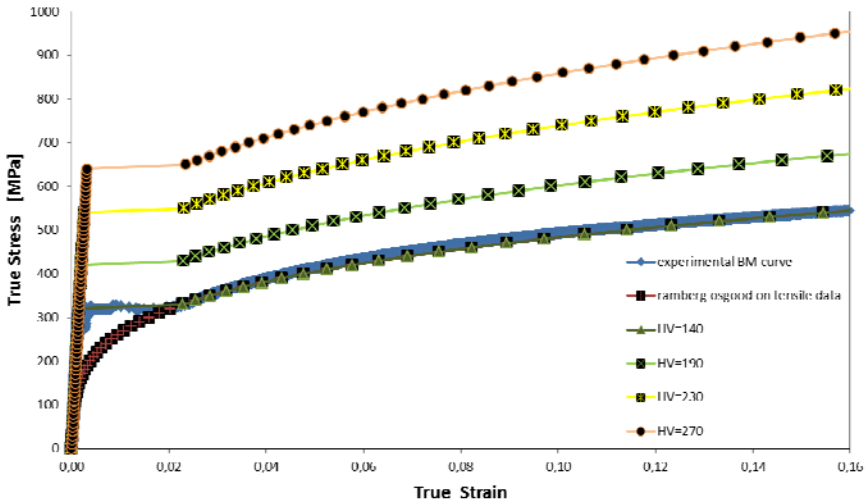


Figure 6: True stress-strain curve depending on hardness measurements.

## *Experimental Tests and DIC analysis*

Displacement controlled tests at R=-1 ($u_x$=±1.2 mm) were performed, where x is the vertical direction. The images of the specimen during the tests were acquired and processed by means of the ARAMIS system using the DIC technique. The experimental set-up is shown in Fig. 7. Fig. 8 shows the values of force and displacement, measured in two cycles. It can be noted that the imposed displacement is symmetric, while the measured force has different absolute values at maximum $F_{max}$ and mininum $F_{min}$ loads, due to the structural weakness under compressive load caused by axial misalignment and due to the presence of residual stresses caused by the welding process. Furthermore, the value of $F_{min}$ is not in correspondence of the minimum displacement value, in fact as shown by fig 9, the specimen deforms in a way that bending (buckling) arises causing a diminution of the load. This behavior is also confirmed by the DIC analysis, shown in Fig. 10 and 11, which illustrate the strain in the x–direction $\varepsilon_x$ (vertical longitudinal direction) at $F_{max}$ and $F_{min}$, respectively. Fig. 10 shows a difference in terms of $\varepsilon_x$ from the left side (about 1%) to the right side (about 0.5%), which means that not only tensile stresses are occurring, but there is also a bending component. This effect is increased under compressive loads in Fig. 11, which exhibits negative and positive strains respectively of +1.2 and -1.2%. The DIC results, shown in Fig. 10 and 11, illustrate that large strains occur close to the notch and they become even larger along the base material.

Figure 7: Experimental setup.

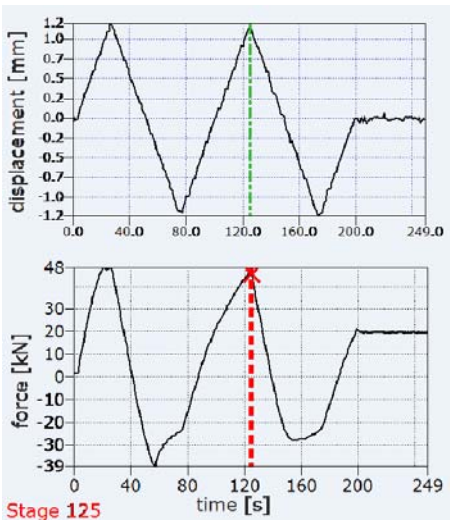


Figure 8: Imposed displacement and measured force.

Figure 9: Deformed specimen at $F_{min}$.

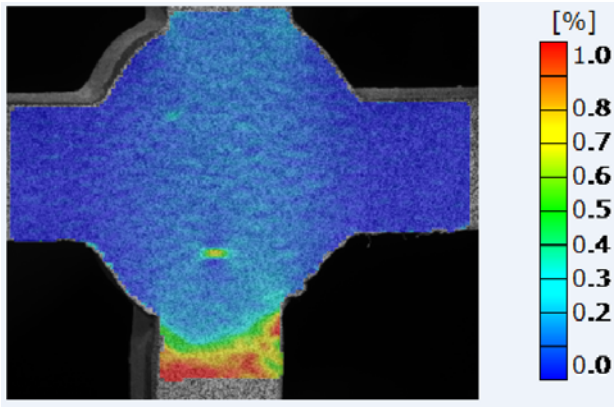


Figure 10: $\varepsilon_x$ at $F_{max}$ ($u_x$ = 1.2 mm).

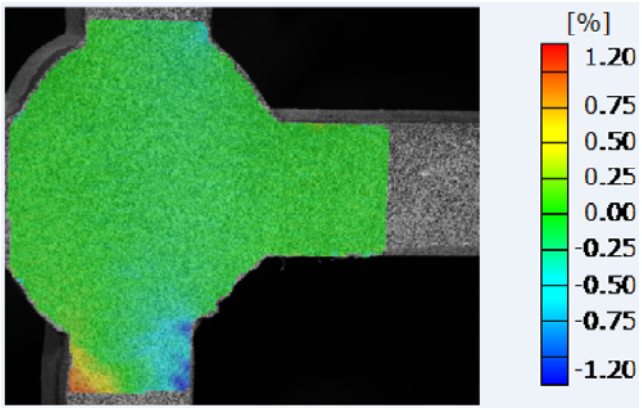


Figure 11: $\varepsilon_x$ at $F_{min}$ ($u_x$=-1.2 mm).

## *Finite Element Analysis and Comparison to DIC results*

ANSYS software was used for a nonlinear FE analysis of the cruciform welded joint. The mesh elements of the 3D FE model are of type solid186. Fig. 12 shows the local geometry used in the FE model for the welds and the notches, with a notch radius of 1 mm. The minimum size of the element is 0.018 mm in the radial direction, 0.018 mm in the

circumferential direction, and 1.2 mm along the thickness direction. Different material zones (BM, HAZ, WM) were considered in the FE model with their different σ-ε curves according to Fig. 6, no misalignment was considered in the FE model.

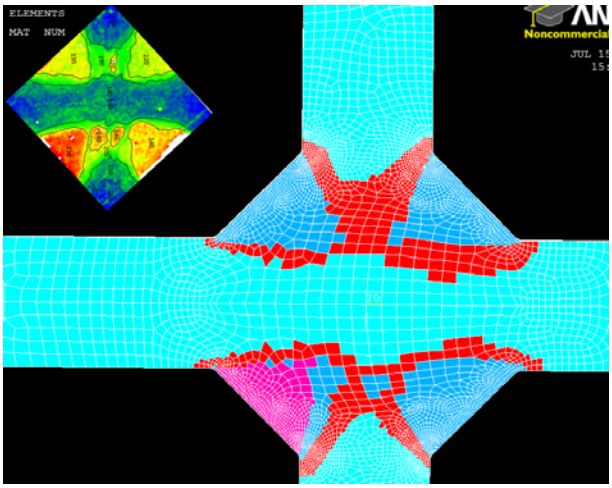


Figure 12: Different material zones defined in the FE model.

A preliminary FE analysis at high nominal stress ($0<\sigma_n<530$ MPa) was performed in order to capture and highlight the influence of the different hardnesses. The geometry and the boundary conditions were the same as in the experimental test, the load is applied to the superior vertical plate, while the inferior vertical plate is clamped. The nominal stress ($\sigma_n$) was determined from the introduced force. Fig. 13 to 15 show the results in terms of strains and stresses in the x direction. In the elastic phase, the values of $\varepsilon_x$ are higher getting closer to the notch, while, as $\sigma_n$ exceeds the $\sigma_y$ value, the strain in the notch depicted in Fig. 15 is higher than that the one in Fig. 13, but it is smaller near the notch than in the base material (excluding the sharp notch). This effect is due to the differences induced by the hardness values to the material characteristics.

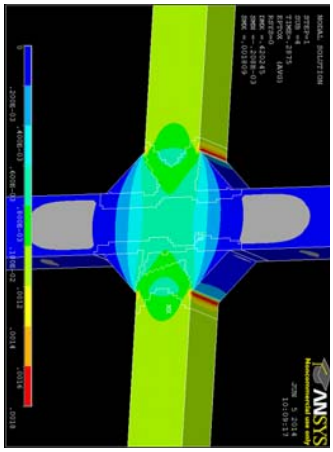

Figure 13: $\varepsilon_x$ for $\sigma_n$ =180 MPa ($\sigma_n < \sigma_y$).

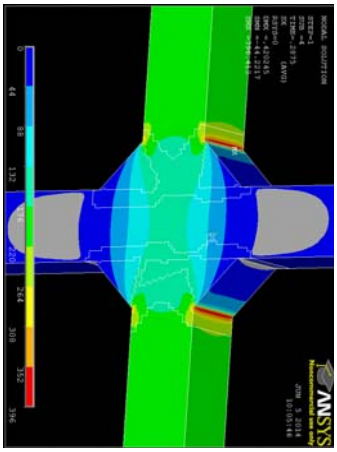

Figure 14: $\sigma_x$ for $\sigma_n$ =180 MPa ($\sigma_n < \sigma_y$).

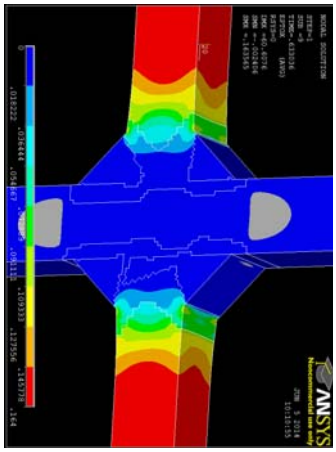

Figure 15: $\varepsilon_x$ for $\sigma_n$ =530 MPa ($\sigma_n > \sigma_y$).

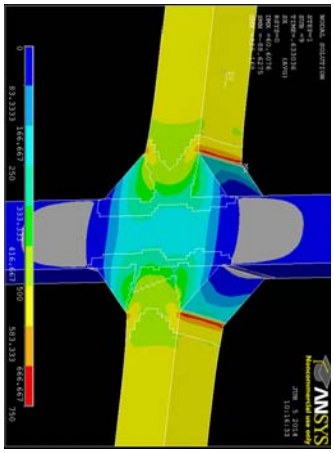

Figure 16: $\sigma_x$ for $\sigma_n$ =530 MPa ($\sigma_n > \sigma_y$).

Moreover, a FE analysis was performed using the same boundary and loading conditions of the experimental tests (the load was introduced by prescribing a displacement of ±1.2 mm to the superior vertical plate). Fig. 17 and 18 show a comparison between the deformed shapes of the real specimen and the FE model at $F_{min}$. Fig. 19 and 20 confirm the result of the experimental analysis: there are both the components of axial and bending stresses, especially at $F_{min}$. Furthermore, the strains are larger along the base material than in the weld metal.

Figure 17: Deformed shape of specimen at $F_{min}$.

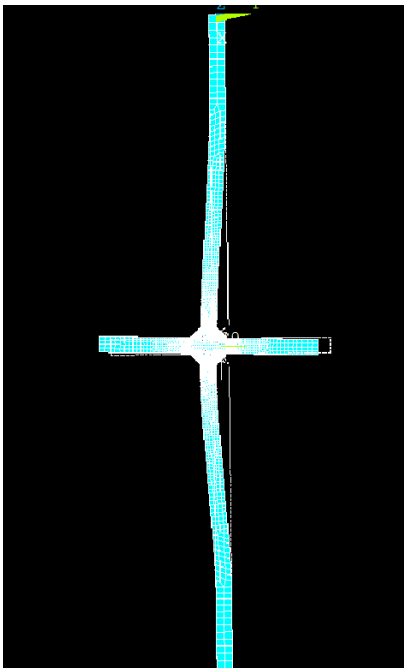

Figure 18: FE deformed shape at $F_{min}$.

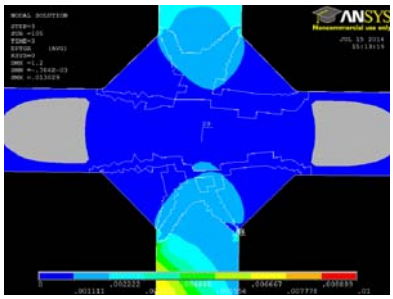

Figure 19: $\varepsilon_x$ at $F_{max}$ ($u_x$ = 1.2 mm).

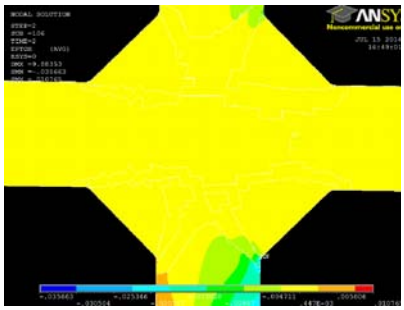

Figure 20: $\varepsilon_x$ at $F_{min}$ ($u_x$=-1.2 mm).

Although the behavior is well represented, the values, in terms of $\varepsilon_x$ at $F_{max}$ and $F_{min}$, differ from the experimental data, due to residual stresses. For this reason a further analysis of the strain range $\Delta\varepsilon_x$, evaluated between $F_{max}$ and $F_{min}$, i.e. after relaxation during initial loading, was done and the results were compared with DIC data, as shown in Fig. 21. The comparison, in this case, shows a general good agreement, but the FE analysis exhibits larger strains in the notch proximity.

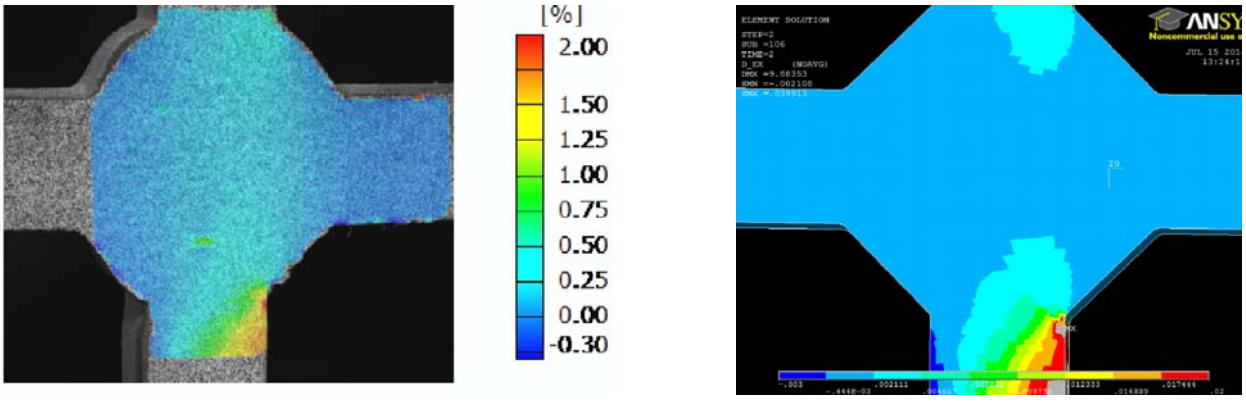


Figure 21: DIC vs FE values of $\Delta\varepsilon_x$.

## Conclusions

A procedure was developed to analyze the response of the investigated cruciform welded joint under static loading. It is based on the following steps: the hardness measurements, using an innovative method for the identification of the different zones (BM, HAZ, and WM) and the assessment of their constitutive curves, the realization of a nonlinear finite element analysis considering the different material properties and, finally, the validation of FE model by means of the experimental data, obtained by DIC technique.
The applied procedure allows providing useful information to the development of models for the prediction of fracture behaviour of the welded joints also under fatigue loading.

## AKNOWLEDGMENTS

The authors are grateful to the Institute of Materials Research, Materials Mechanics, Solid-State Joining Processes at the Helmholtz-Zentrum Geesthacht in Germany for the technical support and the efficient cooperation during the hardness measurements.

## REFERENCES

[1] Fricke, W., Recent Developments and Future Challenges in Fatigue Strength Assessment of Welded Joints, accepted for publication in the Special Issue, Fatigue Design and Analysis in Transportation Engineering, P I Mech. Eng. C – J. Mec, (2015).
[2] Radaj, D., Sonsino, C.M., Fricke, W., Fatigue Assessment of Welded Joints by Local Approaches. Cambridge: Woodhead Publ Series in Welding and Other Joining Technologies, 59 (2006).
[3] ASM Metals Handbook, Welding, Brazing and Soldering, ASM International, 6 (1993).
[4] Crupi, V., Guglielmino, E., Risitano, A., Taylor, D., Different methods for fatigue assessment of T welded joints used in ship structures, J. Ship Res, 51 (2) (2007) 150-159.
[5] Crupi, V, Chiofalo, G., Guglielmino, E., Using Infrared Thermography in Low-Cycle Fatigue Studies of Welded Joints. Weld J, 89(9) (2010) 195 – 200.
[6] Susmel, L., Multiaxial Notch Fatigue: from nominal to local stress-strain quantities. Woodhead & CRC, Cambridge, UK, (2009).
[7] Susmel, L., Nominal stresses and Modified Wöhler Curve Method to perform the fatigue assessment of uniaxially loaded inclined welds, accepted for the publication on the Special Issue, Fatigue Design and Analysis in Transportation Engineering, P I Mech. Eng. C – J. Mec, (2015).
[8] Atzori, B., Lazzarin, P., Meneghetti, G., Ricotta, M., Fatigue design of complex welded structures, Int J Fatigue, 31 (2009) 59–69.
[9] Lopez, Z., Fatemi, A., A method of predicting cyclic stress-strain curve from tensile properties for steels, Mat Sci Eng A-Struct, 556 (2012) 540–550.